Polyhedron 213 (2022) 115551

Contents lists available at ScienceDirect

Polyhedron

journal homepage: www.elsevier.com/locate/poly

A heterometallic [Mn_9Ni_2] cluster consisting of the [$M_4(\mu_3\text{-}O)_3(\mu_3\text{-}Cl)]^{n+}$ cubane and [$Mn^{III}{}_3(\mu_3\text{-}O)_4]^+$ "V-shaped" sub-units appearing in the giant [Mn_{84}] and [Mn_{70}] compounds and its [$Mn_9Co^{III}{}_2$] analogue☆

Eleni E. Moushi [a], Maria Charalambous [b], Constantina Papatriantafyllopoulou [c,1], George Christou [c], Anastasios J. Tasiopoulos [b,*]

[a] Department of Life Sciences, School of Science, European University Cyprus, 1516 Nicosia, Cyprus
[b] Department of Chemistry, University of Cyprus, 1678 Nicosia, Cyprus
[c] Department of Chemistry, University of Florida, Gainesville, FL 32611, USA

ARTICLE INFO

Keywords:
Manganese clusters
Heterometallic clusters
Crystal structures
Magnetic properties
Single-molecule magnets

ABSTRACT

Two new heterometallic clusters exhibiting related cores, [$Mn_9Ni_2(\mu_3\text{-}O)_{10}(\mu_3\text{-}Cl)_2(O_2CMe)_{11}(py)_4(H_2O)_4]\cdot 2H_2O$ (**1**·$2H_2O$) (py = pyridine) and [$Mn_9Co_2(\mu_3\text{-}O)_{10}(\mu_3\text{-}OH)_2(O_2CEt)_{10}(EtOH)_3(H_2O)(py)_5](ClO_4)_2Cl$ (**2**) are reported. Compounds **1**·$2H_2O$/**2** were prepared from reactions of [$Mn_3O(O_2CMe)_6(py)_3]\cdot py$/[$Mn_3O(O_2CEt)_6(py)_3](ClO_4)$ with $MCl_2\cdot 6H_2O$ (M = Ni^{2+}, Co^{2+}) and ($Bu^n{}_4N)MnO_4$ in a 1:3:0.1/1:1:0.1 molar ratio in MeCN (15 ml)/MeOH-EtOH (15–0.5 ml) in ~ 28 %/< 2 % yields, respectively. Their cores consist of two [$Mn^{IV}Mn^{III}{}_2M^{n+}(\mu_3\text{-}O)_3(\mu_3\text{-}X)]^{m+}$ cubanes (M^{n+} = Ni^{2+}, X = Cl^-, m = 5+, **1**·$2H_2O$; M^{n+} = Co^{3+}, X = OH^-, m = 6+, **2**) at the terminal positions linked through a central [$Mn^{III}{}_3(\mu_3\text{-}O)_4]^+$ slightly V-shaped sub-unit. Interestingly, this core has appeared as a fragment in the giant [Mn_{84}] and [Mn_{70}] torus–like single–molecule magnets (SMMs). Magnetism studies of **1**·$2H_2O$ revealed the presence of competing ferromagnetic and antiferromagnetic exchange interactions leading to a fairly low spin ground state value of $S_T \approx 4$ or 3 and fully visible out-of-phase ac signals (above 1.8 K) indicative of slow relaxation of the magnetization and SMM behavior.

1. Introduction

Polynuclear clusters of paramagnetic 3d metal ions have attracted significant attention because of their fascinating crystal structures and interesting magnetic properties. [1–5] In particular, they often display aesthetically pleasing crystal structures with novel characteristics including large size, high nuclearities and, high symmetry structural cores. [1] In addition, they sometimes exhibit unusual magnetic properties with several of them displaying ferromagnetic exchange interactions between their metal ions, large spin ground state values, and single-molecule magnetism (SMM) behavior. [2–10] For this reason there have been continuing efforts focusing on the development of new synthetic methods leading to high nuclearity clusters [5–7].

Apart from the large size and high nuclearities, polynuclear complexes also exhibit additional interesting structural features that have attracted the attention of research community. These include their similarity with various inorganic solids such as a variety of metal oxides/hydroxides, [11–14] polyoxometallates, [15–17] perovskites, [18] etc. In addition, significant attention has been attracted to the construction of high nuclearity compounds based on oligonuclear sub-units and the identification/isolation in a discrete form of oligonuclear building units appearing in polynuclear aggregates. For example, several polynuclear clusters including wheels, disks, rods and others have been reported based on oxido-centered triangles, [19–22] tetranuclear cubanes [23] and other oligonuclear complexes. [24] The isolation of such compounds may provide information about the synthetic steps and intermediates that lead to the formation and aggregation of selected oligonuclear units and about how the overall magnetic behavior of the high nuclearity compounds is affected by the presence of these units. Another interesting example of an oligonuclear unit appearing fairly often in Mn cluster chemistry either in a discrete form [25] or as a fragment of high nuclearity clusters [9,10,23,26,27] is the

☆ Part of the special issue dedicated to the element manganese, entitled *Manganese: A Tribute to Chemical Diversity*.

* Corresponding author.
E-mail address: atasio@ucy.ac.cy (A.J. Tasiopoulos).
[1] Current address: School of Chemistry, College of Science and Engineering, National University of Ireland Galway, H91 TK33, Galway, Ireland.

https://doi.org/10.1016/j.poly.2021.115551
Received 7 August 2021; Accepted 22 October 2021
Available online 6 November 2021

$[Mn^{III}_6Mn^{II}_4(\mu_4\text{-}O)_4]^{18+}$ supertetrahedron. Selected examples of high nuclearity clusters based on this unit are the $[Mn_{17}]$, [10] $[Mn_{25}Na_4]$ and $[Mn_{49}]$ [24] aggregates consisting of two, four and eight edge-sharing decametallic supertetrahedra, respectively. In addition, the same repeating sub-unit has appeared in the family of $[Mn_{36}Ni_4]$ and $[Mn_{32}Co_8]$ "loops-of-loops-and-supertetrahedra" aggregates consisting of two loops and two supertetrahedra. [26,27] Interestingly, in all cases the decametallic supertetrahedral sub-unit affected dramatically the magnetic properties of these compounds since they all display dominant (or entirely in the case of $[Mn_{17}]$) ferromagnetic exchange interactions, large spin ground states, up to $S_T = 37$ in the case of the $[Mn_{17}]$ cluster, and very small zero – field splitting parameter, D (as a result of its highly symmetric structure).

Another family of compounds that has attracted significant attention mainly because of their high nuclearity and size are the giant $[Mn_{84}]$ and $[Mn_{70}]$ compounds exhibiting a torus structure with outer/cavity diameters of 4.2/1.9 Å and 3.7/1.4 Å, respectively. [28,29] They are based on alternating $[Mn^{III}_4(\mu_3\text{-}O)_4]^{4+}$ cubanes and $[Mn^{III}_3(\mu_3\text{-}O)_4]^{+}$ "V-shaped" sub-units with the asymmetric unit of $[Mn_{84}]$ being a $[Mn_{14}]$ cluster consisting of two pairs of alternating $[Mn_4]/[Mn_3]$ sub-units. These compounds exhibit SMM behavior with U_{eff} = 18 K ($[Mn_{84}]$) and 23 K ($[Mn_{70}\text{-OEt}]$), and are the highest nuclearity Mn clusters and SMMs.

Herein we report the synthesis and crystal structures of the heterometallic clusters $[Mn_9Ni_2(\mu_3\text{-}O)_{10}(\mu_3\text{-}Cl)_2(O_2CMe)_{11}(py)_4(H_2O)_4]$ (**1**) (py = pyridine) and $[Mn_9Co_2(\mu_3\text{-}O)_{10}(\mu_3\text{-}OH)_2(O_2CEt)_{10}(EtOH)_3(H_2O)(py)_5](ClO_4)_2Cl$ (**2**) consisting of two $[Mn^{IV}Mn^{III}_2M^{n+}(\mu_3\text{-}O)_3(\mu_3\text{-}X)]^{m+}$ cubanes ($M^{n+} = Ni^{2+}$, X = Cl^-, m = 5+, **1**; $M^{n+} = Co^{3+}$, X = OH^-, m = 6+, **2**) linked through a $[Mn^{III}_3(\mu_3\text{-}O)_4]^{+}$ "V-shaped" sub-unit. These two compounds are similar to a fragment of the giant $[Mn_{84}]$ and $[Mn_{70}]$ wheels since they consist of related repeating oligonuclear units. Magnetism studies of compound **1**·2H_2O revealed the presence of competing ferromagnetic and antiferromagnetic exchange interactions and a spin ground state value $S_T \approx 4$ or 3. Ac studies revealed the presence of fully visible above 1.8 K out-of-phase ac signals and a U_{eff} value ≈ 15 K.

2. Materials and methods

All manipulations were performed under aerobic conditions using materials (reagent grade) and solvents as received. $[Mn_3O(O_2CMe)_6(py)_3]\cdot py$, $[Mn_3O(O_2CEt)_6(py)_3](ClO_4)$ and $(Bu^n_4N)MnO_4$ were prepared as described elsewhere. [30–32]

2.1. Compound preparation

2.1.1. $[Mn_9Ni_2(\mu_3\text{-}O)_{10}(\mu_3\text{-}Cl)_2(O_2CMe)_{11}(py)_4(H_2O)_4]$ (1)

Method A: To a stirred solution of $[Mn_3O(O_2CMe)_6(py)_3]\cdot py$ (0.14 g, 0.17 mmol) in MeCN (15 ml) were added solid $NiCl_2\cdot 6H_2O$ (0.12 g, 0.50 mmol) and $(Bu^n_4N)N_3$ (0.05 g, 0.17 mmol), and the resulting solution was stirred for ~ 1.5 hr. The yellowish-brown solution was filtered, and the filtrate left undisturbed at room temperature in a closed flask. After one week, X-ray quality, brown, polyhedral-shaped crystals of compound **1**·2H_2O were obtained. The crystals were collected by filtration, washed with cold MeCN and dried under vacuum. The reaction yield was ~ 28% based on total Mn content. The dried solid analyzed satisfactorily as **1**·2H_2O ($C_{42}H_{65}N_4O_{38}Cl_2Mn_9Ni_2$): Anal. Calc.: C 26.32; H 3.42; N 2.92; Found: C 26.52; H 3.17; N 3.21. Mn and Ni analysis of the dried solid was performed by inductively coupled plasma optical emission spectrometry (ICP-OES). Anal. Calc. for **1**·2H_2O: Mn 25.80; Ni 6.12; Found: Mn 26.15; Ni 5.90. Selected IR data: (KBr): $\tilde{\nu}$ (cm^{-1}) = 3429(m, br), 1529(s, br), 1413(s, br), 1045(w), 640 (s, br).

Method B: Method A was repeated using $(Bu^n_4N)MnO_4$ (0.007 g, 0.017 mmol) instead of $(Bu^n_4N)N_3$. The resulting brown mixture was filtered and after one week brown, polyhedral-shaped crystals of **1**·2H_2O were observed. The yield was ~ 29%.

Table 1
Selected crystal data for **1** and **2**.

Empirical formula	$C_{42}H_{53}Cl_2Mn_9N_4Ni_2O_{36}$	$C_{61}H_{97}Cl_2Co_2Mn_9N_5O_{40}$
Formula weight	1872.66	2223.65
Temperature (K)	100(2)	100(2)
Wavelength (Å)	1.54184	0.71073 Å
Crystal system	Orthorhombic	Monoclinic
Space group	*Pnma*	P $2_1/n$
Unit cell dimensions	a = 23.9117(9) Å b = 29.5063(6) Å c = 10.3785(4) Å	a = 13.4853(2) Å b = 24.9254(4) Å c = 26.2398(4) Å β = 92.818 (2)°
Volume ($Å^3$)	7322.5(4)	8809.2(2)
Z	4	4
Density (calculated)(g/cm^3)	1.699	1.677
F(000)	3744	4524
Crystal size (mm^3)	0.08 × 0.03 × 0.01	0.24 × 0.08 × 0.05
θ range for data collection (°)	2.995 to 73.028	3.109 to 24.999
Index ranges	$-29\le h\le 27$, $-28\le k\le 36$, $-12\le l\le 12$	$-15\le h\le 16$, $-29\le k\le 18$, $-29\le l\le 31$
Reflections collected	30418	37405
Independent reflections	7350 [R_{int} = 0.0631]	15436 [R_{int} = 0.0364]
Completeness to θ = 67.684° (1) 24.999° (2)	0.985	0.995
Refinement method	Full-matrix least-squares on F^2	Full-matrix least-squares on F^2
Data/restraints/parameters	7350/96/445	15436/49/1174
Goodness-of-fit	1.727	1.043
Final R indices [I > 2σ(I)]	R_{obs}[a] = 0.0967, wR_{obs}[b] = 0.2264	R_{obs}[a] = 0.0373, wR_{obs}[b] = 0.0909
R indices [all data]	R_{all}[a] = 0.1266, wR_{all}[b] = 0.2432	R_{all}[a] = 0.0468, wR_{all}[b] = 0.0951
Largest diff. peak and hole	1.907 and −1.940 e·$Å^{-3}$	0.811 and −0.474 e·$Å^{-3}$

[a] $R = \Sigma||F_o|-|F_c||/\Sigma|F_o|$, [b] $wR = \{\Sigma[w(|F_o|^2 - |F_c|^2)^2]/\Sigma[w(|F_o|^4)]\}^{1/2}$ and $w = 1/[\sigma^2(Fo^2)+(mP)^2 + nP]$ where $P=(Fo^2 + 2Fc^2)/3$ and m and n are constants.

2.1.2. $[Mn_9Co_2(\mu_3\text{-}O)_{10}(\mu_3\text{-}OH)_2(O_2CEt)_{10}(EtOH)_3(H_2O)(py)_5](ClO_4)_2Cl$ (2)

To a stirred solution of $[Mn_3O(O_2CEt)_6(py)_3](ClO_4)$ (0.20 g, 0.21 mmol) in MeOH/EtOH (15/0.5 ml) were added solid $CoCl_2\cdot 6H_2O$ (0.05 g, 0.21 mmol) and $(Bu^n_4N)MnO_4$ (0.008 g, 0.021 mmol), and the resulting dark brown solution was stirred for 2 h. Then the solution was filtered and the filtrate maintained undisturbed at room temperature in a closed flask. After two weeks, a few X-ray quality, dark brown, polyhedral-shaped crystals of compound **2** were observed. The crystals were collected by filtration, washed with cold MeOH and dried under vacuum. The reaction yield was < 2% based on total Mn content.

2.2. Physical measurements

Microanalyses (C, H, N) were performed by the in-house facilities of the University of Florida, Chemistry Department. IR spectra (4000–400 cm^{-1}) were recorded on a Shimadzu Prestige-21 spectrometer with the samples prepared as KBr pellets. Variable-temperature dc and ac magnetic susceptibility data were collected at the University of Florida using a Quantum Design MPMS-XL SQUID instrument equipped with a 7 T magnet and operating in the 1.8–300 K range. Samples were embedded in solid eicosane to prevent torquing. The ac magnetic susceptibility measurements were performed in an oscillating ac field of 3.5 G and a zero dc field. Pascal's constants were used to estimate the diamagnetic corrections, which were subtracted from the experimental susceptibilities to give the molar paramagnetic susceptibility (χ_M).

2.2.1. Single-crystal X-ray crystallography

Single-crystal X-ray diffraction data were collected on a Rigaku

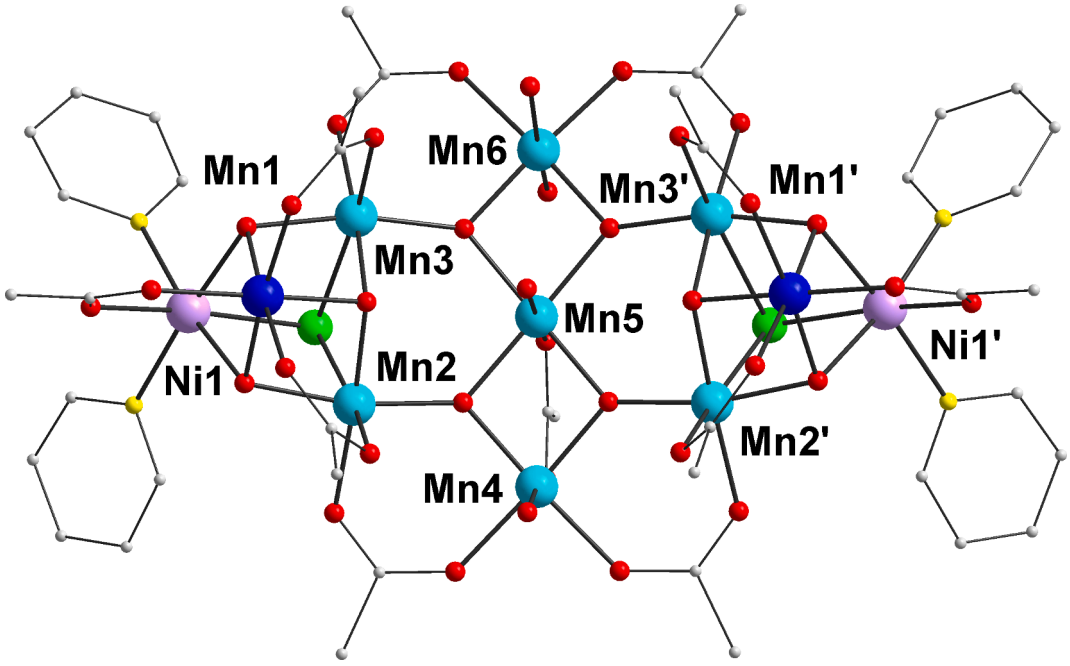

Fig. 1. Partially labeled representation[a] of the molecular structure of complex **1**. Color code: Mn^{IV}, blue; Mn^{III}, turquoise; Ni, lavender; Cl, green; O, red; N, yellow; C, grey. The hydrogen atoms are omitted for clarity. [a] Symmetry code: (′) = *x*, 1.5-y, z.

Supernova A X-ray diffractometer, equipped with a CCD area detector and a graphite monochromator utilizing Cu-Ka (λ = 1.54184 Å) and Mo-Ka radiation (λ = 0.71073 Å) for **1** and **2**, respectively. Suitable crystals covered with paratone-N oil were mounted on the tip of glass fibers or scooped up in cryo-loops at the end of a copper pin and transferred to a goniostat where they were cooled for data collection. Empirical absorption corrections (multi-scan based on symmetry-related measurements) were applied using CrysAlisRED software. [33] Software packages used: CrysAlisCCD for data collection, CrysAlisRED for cell refinement and data reduction, [33] SHELXL for structure solution, [34] WINGX for geometric calculations, [35] while DIAMOND [36] and MERCURY [37] were used for molecular graphics. The non-H atoms were treated anisotropically, whereas the aromatic hydrogen atoms were placed in calculated, ideal positions and refined as riding on their respective carbon atoms. Electron density contributions from disordered guest molecules including one ClO_4^- counter-anion of **2** that was located but could not be modelled properly were handled using the SQUEEZE procedure from the PLATON software suit. [38] In order to limit the disorder of bridging carboxylate (in **1** and **2**) and EtOH terminal ligands (in **2**), various restraints (DFIX, DELU, SIMU, ISOR) have been applied in the refinement of the crystal structures. Selected crystal data for **1** and **2** are summarized in Table 1.

3. Results and discussion

3.1. Synthesis

Our group has been investigating reactions of Mn reagents with other 3d metal compounds targeting mixed Mn/M (M = 3d metal ion) clusters. This approach has proven successful, especially for the synthesis of mixed Mn/Ni clusters, and led to a variety of new heterometallic clusters. Some examples of such Mn/Ni heterometallic clusters are the high nuclearity $[Mn^{IV}{}_{12}Mn^{III}{}_{12}Ni^{II}{}_2O_{30}(O_2CEt)_{16}(MeO)_{12}(MeOH)_8(H_2O)_2]$ ($[Mn_{24}Ni_2]$) consisting of a $[Mn^{III}{}_{12}Ni_2]$ loop incorporating a $[Mn^{IV}{}_{12}]$ [3 × 4] grid-like unit, [39] and the $[Mn^{III}{}_2Ni^{II}{}_6(\mu_4\text{-}O)_2(\mu_3\text{-}OH)_4(\mu_3\text{-}Cl)_2(O_2CMe)_6(py)_8]^{2+}$ ($[Mn_2Ni_6]$) cluster containing two $[Mn^{III}Ni^{II}{}_3]$ cubanes linked through oxide and carboxylate ligands. [26] These compounds were prepared from reactions of an oxido-centered Mn triangle with $NiCl_2{\cdot}6H_2O$ and an oxidant or a salt in an alcohol (for $[Mn_{24}Ni_2]$: $[Mn_3O(O_2CEt)_6(py)_3]ClO_4$, $Bu^n{}_4NMnO_4$, MeOH; for $[Mn_2Ni_6]$: $[Mn_3O(O_2CMe)_6(py)_3]{\cdot}py$, $NaClO_4$, EtOH). Compound **1** was prepared from modifications of the above reaction scheme that included use of various different salts and solvents. In particular, the reaction of $[Mn_3O(O_2CMe)_6(py)_3]{\cdot}py$ with $NiCl_2{\cdot}6H_2O$ and $(Bu^n{}_4N)N_3$ in a 1:3:1 molar ratio in MeCN afforded compound $\mathbf{1}{\cdot}2H_2O$ in ~ 28% yield based on total Mn content. It was noted that the average oxidation state of the Mn ions in the reaction mixture ($Mn^{III}{}_2Mn^{II}$; 2.66) was lower that the corresponding value in the isolated product ($Mn^{IV}{}_2Mn^{III}{}_7$; 3.22); the oxidizing agent in this reaction was probably atmospheric O_2 or a disproportionation. For this reason, and because none of the ions of $(Bu^n{}_4N)N_3$ are present in the structure of $\mathbf{1}{\cdot}2H_2O$, we repeated the same reaction using $(Bu^n{}_4N)MnO_4$ in place of $(Bu^n{}_4N)N_3$ targeting an improvement in the reaction yield. However, although compound $\mathbf{1}{\cdot}2H_2O$ was successfully synthesized with this procedure, the reaction yield was not improved. The formation of compound **1** is summarized in Eq. (1):

$$3\left[Mn_3O(O_2CMe)_6(py)_3\right]{\cdot}py + 2NiCl_2{\cdot}6H_2O + 1.25O_2 \xrightarrow{MeCN} [\boldsymbol{Mn_9Ni_2O_{10}Cl_2(O_2CMe)_{11}(py)_4(H_2O)_4}]{\cdot}\mathbf{2H_2O} + 2HCl + 8py + 7CH_3COOH + 1.5H_2O \quad (1)$$

Several other modifications were performed to the reaction that afforded $\mathbf{1}{\cdot}2H_2O$ targeting the isolation of additional heterometallic $[Mn_9M_2]$ analogues. These involved variations in the $MCl_2{\cdot}xH_2O$ salts of different 3d metal ions, the oxido-centered Mn triangles (involving use of triangles possessing different carboxylate groups), the solvents, etc. Thus, the reaction of $[Mn_3O(O_2CEt)_6(py)_3](ClO_4)$ with $CoCl_2{\cdot}6H_2O$ and $(Bu^n{}_4N)MnO_4$ in 1:1:0.1 M ratio in MeOH afforded a few single crystals of compound **2**, which allowed the determination of its crystal structure. However, several other attempts to obtain this compound by employing this reaction did not succeed. The crystal structure of **2** revealed the presence of coordinated EtOH molecules. This solvent was not used in the reaction mixture but appeared in the compound probably due to its existence in the lattice of $[Mn_3O(O_2CEt)_6(py)_3]ClO_4$ (its synthesis takes place in EtOH). [31] Thus, the same reaction was repeated in MeOH in the presence of 0.5 ml EtOH affording a few crystals of **2**. The isolation of compound **2** was reproducible, however the reaction yield was very low (<2%) and despite several attempts to increase it, this was not achieved.

For this reason, the compound was not further characterized.

3.2. Description of structures

Representations of the molecular structure of compound **1** are shown in Fig. 1 and S1 in Supplementary information, SI and selected interatomic distances and angles are listed in Table 2.

Complex **1** (Fig. 1 and S1) crystallizes in the orthorhombic space group *Pnma* and its asymmetric unit consists of one half of the $[Mn^{IV}_2Mn^{III}_7Ni^{II}_2]$ cluster. Its $[Mn^{IV}_2Mn^{III}_7Ni^{II}_2(\mu_3\text{-}O)_{10}(\mu_3\text{-}Cl)_2]^{11+}$ structural core consists of two mixed metal $[Mn^{IV}Mn^{III}_2Ni^{II}(\mu_3\text{-}O)_3(\mu_3\text{-}Cl)]^{5+}$ cubanes connected through a "V-shaped" $[Mn^{III}_3(\mu_3\text{-}O)_4]^{+}$ sub-unit. The oxidation states of the Mn ions [40] and the protonation levels of the O atoms [41] were determined by bond valence sum (BVS) calculations (Table S1 in SI), charge considerations, and inspection of metric parameters. All metal ions are hexacoordinated with the Mn^{III} ions possessing distorted octahedral coordination geometry and exhibiting the expected (for high spin d^4 ions) Jahn–Teller (JT) elongations (the JT axes are not co-parallel) (Fig. S2 in SI). The three Mn and one Ni ions of each cubane sub-unit are connected by three $\mu_3\text{-}O^{2-}$ and one $\mu_3\text{-}Cl^{-}$ anions forming the $[Mn^{IV}Mn^{III}_2Ni(\mu_3\text{-}O)_3(\mu_3\text{-}Cl)]^{5+}$ core. The Mn^{IV} ion of the cubane (Mn1) is also linked to the other three metal ions through three acetate ligands bridging in the common *syn,syn*-η^1:η^1:μ coordination mode. In addition, the two Mn^{III} ions of the cubane are linked to the central $[Mn^{III}_3]$ sub-unit through two more *syn,syn*-η^1:η^1:μ acetate ligands and two $\mu_3\text{-}O^{2-}$ anions. Each of the latter connects one Mn^{III} ion of each cubane with two Mn^{III} ions of the central $[Mn^{III}_3]$ sub-unit thus forming two vertex – sharing $[Mn^{III}_2O_2]$ rhombs. The Mn ions of one of the rhombs are also bridged by one *syn,syn*-η^1:η^1:μ acetate ligand forming a $[Mn^{III}_2O_2(\mu\text{-}O_2CMe)]^{+}$ unit. The three Mn ions of the $[Mn_3O_4]$ sub-unit are not linear but slightly V-shaped (Mn4-Mn5-Mn6 = 169.4(2)°). The peripheral ligation of complex **1** is completed by terminally ligated solvent molecules and in particular by four pyridine ligands coordinated to the Ni^{2+} ions and four water molecules to the Mn^{III} ions of the V-shaped $[Mn^{III}_3(\mu_3\text{-}O)_4]^{+}$ sub-unit. A close examination of the packing of **1** revealed the existence of intramolecular H – bonding interactions involving the terminal H_2O molecules of the central $[Mn^{III}_3(\mu_3\text{-}O)_4]^{+}$ sub-unit and the O^{2-}/O_2CMe^{-} anions of the cubane. Despite the presence of intramolecular interactions, no significant direct intermolecular interactions between neighboring $[Mn_9Ni_2]$ clusters exist.

Compound **2** crystallizes in the monoclinic space group $P2_1/n$ and its asymmetric unit consists of a $[Mn^{IV}_2Mn^{III}_7Co^{III}_2]$ cluster cation (Fig. 2 and S3) and two ClO_4^{-} and one Cl^{-} counter - anions. Selected interatomic distances and Mn/Co BVS calculations data [40,42] are included

Table 2
Selected bond lengths (Å) for **1**.[a]

Label	Distances	Label	Distances
Ni1-N1	2.085(8)	Mn3-O11	2.184(7)
Ni1-N2	2.077(7)	Mn3-O12	1.962(8)
Ni1-O1	2.125(7)	Mn3-Cl1	2.723(3)
Ni1-O2	2.063(6)	Mn4-O5	1.869(6)
Ni1-O6	2.034(6)	Mn4-O15	1.971(6)
Ni1-Cl1	2.433(3)	Mn4-O17	2.18(2)
Mn1-O1	1.841(7)	Mn4-O20	2.29(2)
Mn1-O2	1.835(7)	Mn4-O5′	1.869(6)
Mn1-O3	1.848(5)	Mn4-O15′	1.971(6)
Mn1-O7	1.963(5)	Mn5-O4	1.916(6)
Mn1-O8	2.004(7)	Mn5-O5	1.902(6)
Mn1-O10	1.993(7)	Mn5-O16	2.20(2)
Mn2-O1	1.901(5)	Mn5-O21	2.321(8)
Mn2-O3	1.902(7)	Mn5-O5′	1.902(6)
Mn2-O5	1.866(5)	Mn5-O4′	1.916(6)
Mn2-O9	2.183(8)	Mn6-O4	1.857(6)
Mn2-O14	1.959(7)	Mn6-O13	1.973(7)
Mn2-Cl1	2.702(3)	Mn6-O18	2.19(2)
Mn3-O2	1.896(5)	Mn6-O19	2.23(2)
Mn3-O3	1.899(7)	Mn6-O4′	1.857(6)
Mn3-O4	1.879(5)	Mn6-O13′	1.973(7)

[a] Symmetry code: (′) = *x*, 1.5-y, z.

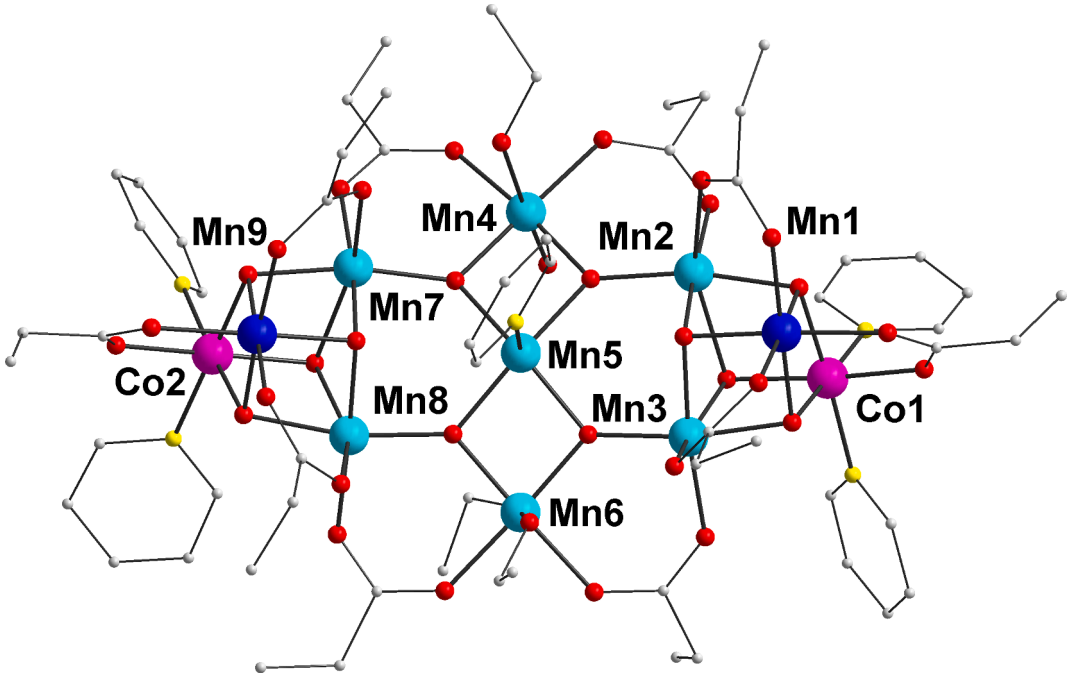

Fig. 2. Partially labeled representation of the molecular structure of complex **2**. Color code: Mn^{IV}, blue; Mn^{III}, turquoise; Co, pink; O, red; N, yellow; C, grey. The hydrogen atoms are omitted for clarity.

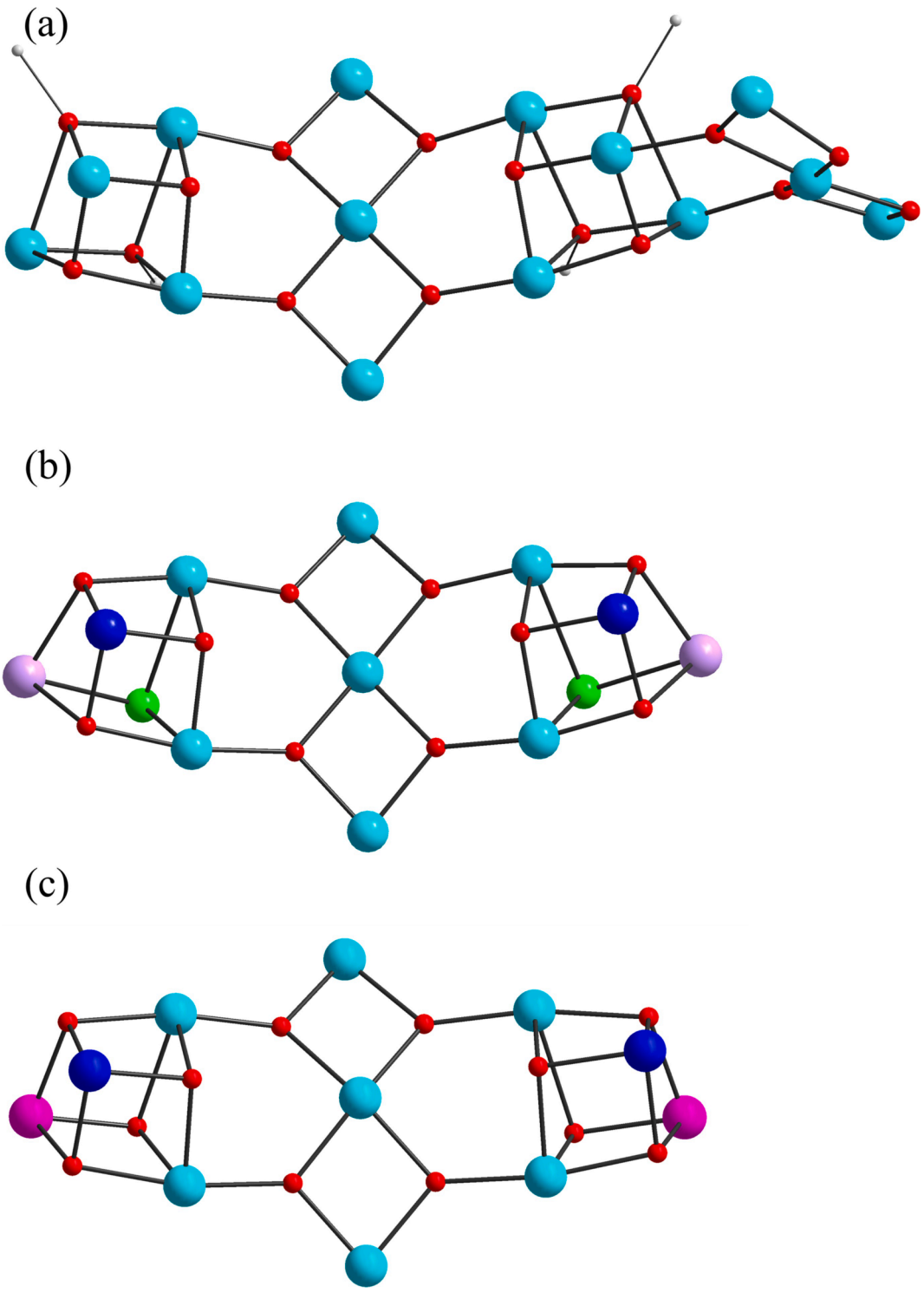

Fig. 3. Representations of the (a) $[Mn^{III}_{14}(\mu_3\text{-}O)_{12}(\mu_3\text{-}OMe)_4]^{14+}$, (b) $[Mn^{IV}_2Mn^{III}_7Ni^{II}_2(\mu_3\text{-}O)_{10}(\mu_3\text{-}Cl)_2]^{11+}$ and (c) $[Mn^{IV}_2Mn^{III}_7Co^{III}_2(\mu_3\text{-}O)_{10}(\mu_3\text{-}OH)_2]^{13+}$ cores of the $[Mn_{14}]$ asymmetric unit of $[Mn_{84}]$ torus–like cluster [28] and compounds **1** and **2**, respectively, emphasizing on their structural similarity. Color code: Mn^{IV}, blue; Mn^{III}, turquoise; Ni, lavender; Co, pink; O, red; Cl, green, C, grey.

in Tables S2 and S3, respectively, in SI.

The $[Mn^{IV}_2Mn^{III}_7Co^{III}_2(\mu_3\text{-}O)_{10}(\mu_3\text{-}OH)_2]^{13+}$ structural core (Fig. 3) consists of two mixed metal $[Mn^{IV}Mn^{III}_2Co^{III}(\mu_3\text{-}O)_3(\mu_3\text{-}OH)]^{6+}$ cubanes connected through a "V-shaped" $[Mn^{III}_3(\mu_3\text{-}O)_4]^{+}$ sub-unit and is related to the $[Mn^{IV}_2Mn^{III}_7Ni^{II}_2(\mu_3\text{-}O)_{10}(\mu_3\text{-}Cl)_2]^{11+}$ core of compound **1** described above (vide supra). For this reason, only the main differences of the structures of compounds **2** and **1** shall be discussed. In particular, the most obvious differences between the two structures involve: (i) the 3d heterometals and their oxidation state values [40,42] (two Co^{III} ions in **2** versus two Ni^{II} ions in **1**); (ii) the type of monoatomic bridging ligands in each cubane sub-unit (three $\mu_3\text{-}O^{2-}$ and one $\mu_3\text{-}OH^{-}$ in **2** versus three $\mu_3\text{-}O^{2-}$ and one $\mu_3\text{-}Cl^{-}$ in **1**); (iii) the type and number of carboxylate ligands (ten O_2CEt ligands in **2** versus eleven O_2CMe ones in **1**; the missing carboxylate group in **2** is the one connecting two Mn ions of the Mn_3O_4 sub-unit); (iv) the number and type of terminal solvent molecules (five py, three EtOH and one H_2O in **2** versus four py and four H_2O molecules in **1**;

and (v) the coordination number and coordination geometry of selected metal ions (all metal ions in **1** are hexacoordinated adopting a distorted octahedral coordination geometry, whereas in **2** the central Mn ion of the $[Mn_3O_4]$ sub-unit is pentacoordinated exhibiting a distorted tetragonal pyramidal coordination geometry). In the case of compound **2** there are also intramolecular interactions involving the EtOH and H_2O terminal solvent molecules of the $[Mn_3O_4]$ sub-unit and the O_2CEt/OH^- ligands and ClO_4^-/Cl^- counter anions but no significant direct intermolecular interactions between neighboring $[Mn_9Co_2]$ clusters was observed.

Compounds **1** and **2** join a small family of undecanuclear Mn-containing clusters, and are unusual examples of heterometallic ones. [43] Their $[Mn_9M_2(\mu_3\text{-}O)_{10}(\mu_3\text{-}X)_2]^{n+}$ (M = Ni^{2+}, X = Cl^-, **1**; M = Co^{3+}, X = OH^-, **2**) structural core or its analogous one $[Mn^{III}_{11}(\mu_3\text{-}O)_8(\mu_3\text{-}OMe)_4]^{13+}$ have appeared previously in a discrete homometallic Mn cluster [44] and also as a fragment of higher nuclearity clusters. In particular, the homometallic $[Mn_{11}(\mu_3\text{-}O)_{10}(\mu_3\text{-}Cl)_2(O_2CMe)_{11}(bpy)_2(\text{-}MeCN)_2(H_2O)_2](ClO_4)_2{\cdot}8MeCN$ (bpy = 2,2′-bipyridyl) $[Mn_{11}]$ displays a $[M^{IV}_2Mn^{III}_9(\mu_3\text{-}O)_{10}(\mu_3\text{-}Cl)_2]^{13+}$ core similar to those of **1** and **2**; however, its magnetic properties have not been investigated. In fact, it would be interesting to study the magnetic properties of this $[Mn_{11}]$ cluster (and of its heterometallic analogues) since it is based on $[Mn^{IV}Mn^{III}_2M^{n+}(\mu_3\text{-}O)_3(\mu_3\text{-}X)]$ (M^{n+} = Mn^{3+}, X = Cl^-, $[Mn_{11}]$ [44]; M = Ni^{2+}, X = Cl^-, **1**; M = Co^{3+}, X = OH^-, **2**) cubanes, which are known to exhibit interesting [45] and sometimes unique [46] magnetic properties. Another reason to prepare and investigate the magnetic properties of compounds consisting of alternating $[Mn_4(\mu_3\text{-}O)_{4\text{-}x}(\mu_3\text{-}X)_x]$ cubane and $[Mn^{III}_3(\mu_3\text{-}O)_4]^+$ V-shaped sub-units is their presence in the family of giant $[Mn_{84}]$ [28] and $[Mn_{70}]$ [29] torus-like clusters exhibiting SMM behavior, which are the highest nuclearity Mn clusters and SMMs reported in the literature. The structural relation of the $[Mn^{IV}_2Mn^{III}_7Ni^{II}_2(\mu_3\text{-}O)_{10}(\mu_3\text{-}Cl)_2]^{11+}$ and $[Mn^{IV}_2Mn^{III}_7Co^{III}_2(\mu_3\text{-}O)_{10}(\mu_3\text{-}OH)_2]^{13+}$ cores of **1** and **2** and the $[Mn^{III}_{14}(\mu_3\text{-}O)_{12}(\mu_3\text{-}OMe)_4]^{14+}$ one of the $[Mn_{84}]$ torus cluster is highlighted in Fig. 3.

3.3. Magnetic properties

Solid-state, variable-temperature magnetic susceptibility measurements were performed on vacuum-dried microcrystalline sample of complex **1**·$2H_2O$ suspended in eicosane to prevent torquing. The dc magnetic susceptibility (χ_M) data were collected in the 5.0–300 K range in a 0.1 T magnetic field and are plotted as $\chi_M T$ *vs* *T* in Fig. 4a.

The $\chi_M T$ for **1**·$2H_2O$ steadily decreases from 19.16 $cm^3\ mol^{-1}$ K at 300 K to 13.41 at 50 K, and then rapidly decreases further to 9.34 $cm^3\ mol^{-1}$ K at 5 K. The 300 K value is lower than the spin-only ($g = 2$) value of 26.75 $cm^3\ mol^{-1}$ K for 2 Mn^{IV}, 7 Mn^{III} and 2 Ni^{II} non-interacting ions, indicating the presence of dominant antiferromagnetic exchange interactions within the molecule. The 5.0 K value is indicative of a small ground-state spin value in the $S = 0 - 4$ range; the spin-only ($g = 2$) values for $S = 1$, 2, 3 and 4 are 1.0, 3.0, 6.0 and 10 $cm^3\ mol^{-1}$ K, respectively.

Given the size of the Mn_9Ni_2 molecule, and the resulting number of inequivalent exchange constants, it is not possible to apply the Kambe method [47] to determine the individual pairwise Mn_2 exchange interaction parameters. Thus, variable field – variable temperature magnetization measurements were performed at applied magnetic fields and temperatures in the 1–40 kG and 1.8–10.0 K range, respectively to obtain additional information concerning the values of the ground-state spin, *S*, and the zero-field splitting parameter, *D*. The data for complex **1**·$2H_2O$ are shown in Fig. 4b, as a reduced magnetization ($M/N\mu_B$) *vs* H/T plot, where *M* is the magnetization, *N* is Avogadro's number, μ_B is the Bohr magneton, and *H* is the magnetic field. For complexes populating only the well-isolated ground state and possessing no axial zero-field splitting (ZFS), i.e. $D = 0$, the magnetization versus field plot follows the Brillouin function and the isofield lines superimpose and saturate at a value of *gS*. However, the experimental data of complex **1**·$2H_2O$ in Fig. 4b clearly do not superimpose, indicating low-lying excited states consistent with the high nuclearity and/or significant magnetic anisotropy (ZFS) in the ground state.

The $M/N\mu_B$ versus H/T data were fit using the program MAGNET to a model that assumes that only the ground state is populated at these temperatures and magnetic fields, includes isotropic Zeeman interactions and axial zero-field splitting ($D\hat{S}_z^2$), and incorporates a full powder average. The corresponding spin Hamiltonian is given by Eq. (1).

$$H = D\hat{S}_z^2 + g\mu_B\mu_0\hat{S}\cdot H \quad (1)$$

where *D* is the axial ZFS parameter, $\hat{S}_z$ is the easy-axis spin operator, μ_0 is the vacuum permeability, and *H* is the applied field. The last term in eq 1 is the Zeeman energy associated with an applied magnetic field. The best fit for **1**·$2H_2O$ is shown as the solid lines in Fig. 4b and was obtained with $S = 4$, $g = 1.83(1)$, $D = -0.57\ cm^{-1}$. Alternative fits with $S = 3$ or 5 were rejected because they gave unreasonable values of *g* and *D*. The *g* value is<2.0, however, it is pointed out that the fit of the reduced magnetization data provides a rough estimation of g and D values; for their accurate determination, additional measurements are required that are

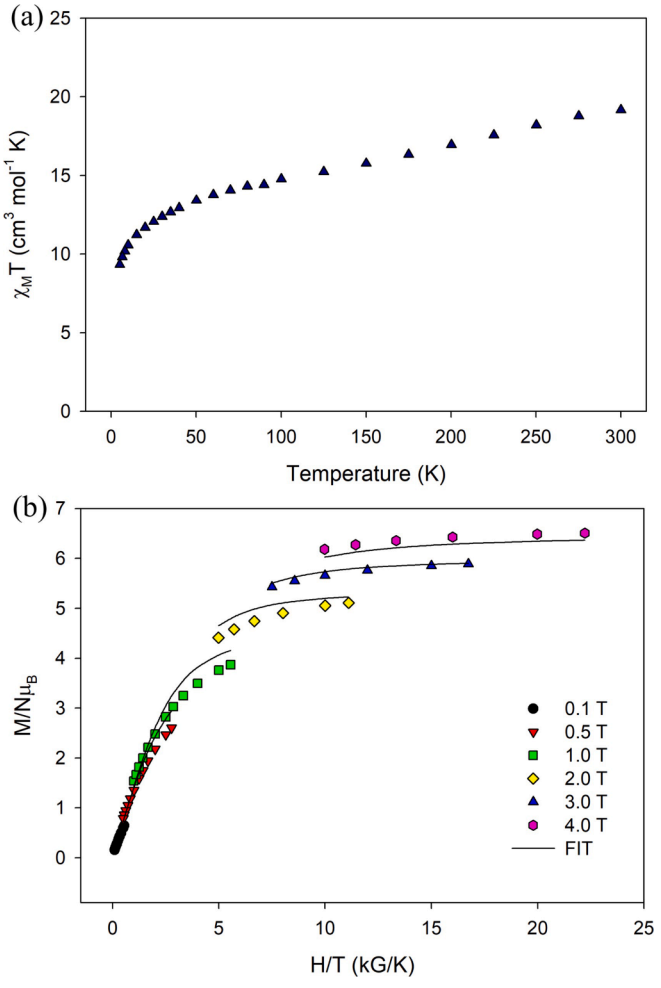

Fig. 4. Plots of (a) $\chi_M T$ *vs* *T* at 0.1 T and (b) reduced magnetization ($M/N\mu_B$) *vs* H/T at the indicated fields for complex **1**·$2H_2O$. The solid lines are the fit of the data; see the text for the fit parameters.

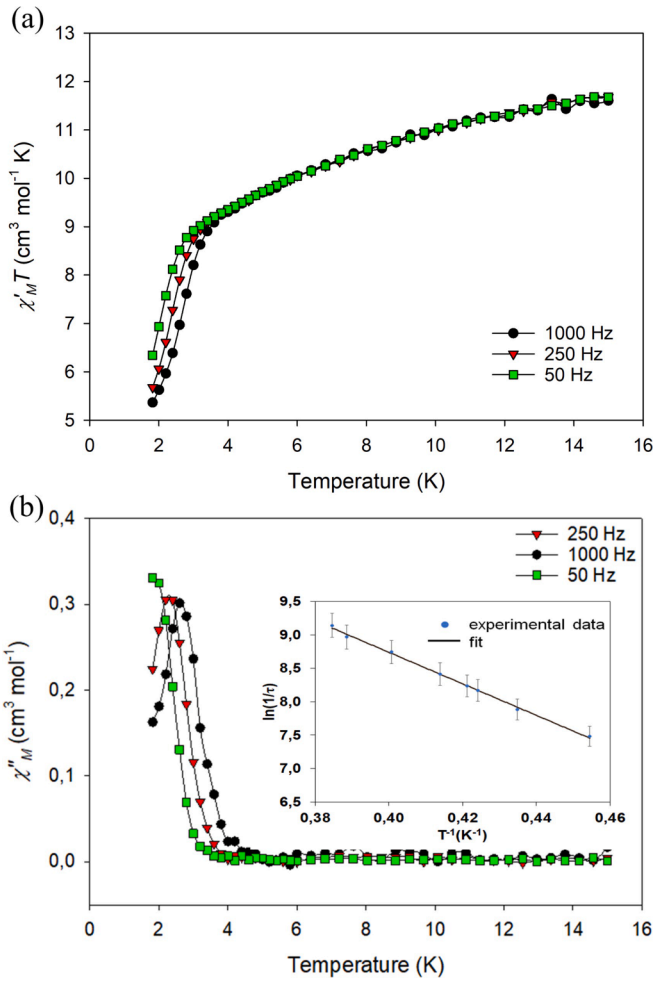

Fig. 5. Plots of (a) the in-phase (χ'_M) signal as $\chi'_M T$ *vs.* T and (b) the out-of-phase (χ''_M) signal as χ''_M *vs.* T in a 3.5 G field oscillating at the indicated frequencies for complex **1**·2H$_2$O. Inset in Fig. 5b: Plot of the natural logarithm of relaxation rate, ln(1/τ), *vs.* inverse temperature (T^{-1}) for **1**·2H$_2$O, using χ'_M *vs.* T data at different frequencies. The solid line is fit to the Arrhenius equation.

beyond the scope of this paper.

Alternating current (ac) magnetic susceptibility data were collected for compound **1**·2H$_2$O to obtain more information about its S_T value and the possibility to exhibit slow relaxation of the magnetization indicative of SMM behavior. The in-phase (Fig. 5a) ac signal displays a decrease in $\chi'_M T$ with lowering of the temperature, assigned to depopulation of low-lying excited states with S greater on average than that of the ground state. It is usually possible to identify the ground state by extrapolating the data to 0 K from a T that avoids other effects such as the onset of slow relaxation or intermolecular interactions; in this case, however, extrapolation of the $\chi'_M T$ data from above ~ 5.0 K to 0 K, at which point only the ground state should be populated, gives a value of ~ 8 cm^3 mol^{-1} K or slightly higher. This corresponds to neither an S = 3 or S = 4 value, and suggests that the excited state(s) is(are) too low-lying for this approach. The combined dc and ac data thus suggest that **1** has either an $S_T \approx 3$ or 4 value. At lower temperatures (below 4 K), there is a frequency-dependent decrease in $\chi'_M T$ and a concomitant appearance of a frequency-dependent out-of-phase (χ''_M) signal (Fig. 5b), indicative of the presence of slow relaxation of the magnetization.

The temperature dependence of the magnetization relaxation rate (1/τ, τ is the relaxation time) was deduced from the out-of-phase χ''_M *vs.* T data collected at multiple frequencies (ν), (Fig. S7). The 1/τ, *vs.* T data were used to construct an Arrhenius plot, shown as ln(1/τ) *vs.* T^{-1} in Fig. 5b, inset, based on the Arrhenius equation (Eq. (2)),

$$1/\tau = (1/\tau_0)\exp(-U_{\text{eff}}/kT) \quad (2)$$

where U_{eff} is the effective energy barrier, k is the Boltzmann constant and $1/\tau_0$ is the pre-exponential factor. The obtained fit parameters were $\tau_0 = 1.3 \times 10^{-10}$ s and $U_{\text{eff}} = 15$ cm^{-1}. The τ_0 is smaller than normally seen for SMMs but this is sometimes the case for higher nuclearity ones. [10,48]

4. Conclusions

The reactions of oxido - centered Mn triangles with NiCl$_2$·6H$_2$O or CoCl$_2$·6H$_2$O in the presence of (Bu$^n_4$N)MnO$_4$ afforded two heterometallic [Mn$^{IV}_2$Mn$^{III}_7$Ni$^{II}_2$] and [Mn$^{IV}_2$Mn$^{III}_7$Co$^{III}_2$] carboxylate clusters. They are based on structurally related [Mn$^{IV}_2$Mn$^{III}_7$M$^{n+}_2$(μ$_3$-O)$_{10}$(μ$_3$-X)$_2$]$^{m+}$ (M^{n+} = Ni^{2+}, X = Cl$^-$, m = +11, **1**; M^{n+} = Co^{3+}, X = OH$^-$, m = +13, **2**) cores consisting of two [Mn^{IV}Mn$^{III}_2$M(μ$_3$-O)$_3$(μ$_3$-X)] cubanes at the terminal positions linked through a central [Mn$^{III}_3$(μ$_3$-O)$_4$]$^+$ slightly V-shaped subunit. Interestingly this core has appeared as a fragment in the giant torus–like [Mn$_{84}$] and [Mn$_{70}$] SMMs. Magnetism studies on compound **1**·2H$_2$O indicated the presence of competing ferromagnetic and antiferromagnetic exchange interaction and a spin ground state value $S_T \approx 4$ or 3. Ac studies revealed the presence of fully visible (above 1.8 K) out-of-phase signals indicating that compound **1**·2H$_2$O is a new SMM with a $U_{\text{eff}} = 15$ cm^{-1}. Compounds **1**·2H$_2$O and **2** are new additions in the family of heterometallic mixed Mn/M (M = a 3d metal ion) clusters that contain carboxylates as the only type of organic bridging ligands establishing Mn/3d metal ion cluster chemistry as source of high nuclearity clusters with aesthetically pleasing structures and interesting magnetic properties. Further studies in this area will involve attempts to synthesize the homometallic [Mn$_{11}$] analogue and also other heterometallic [Mn$_9$M$_2$] clusters with 3d and 4f metal ions.

CRediT authorship contribution statement

Eleni E. Moushi: Investigation, Methodology, Writing – original draft. **Maria Charalambous:** Investigation, Methodology. **Constantina Papatriantafyllopoulou:** Investigation, Methodology. **George Christou:** Investigation, Methodology, Writing – review & editing. **Anastasios J. Tasiopoulos:** Supervision, Writing – review & editing.

Declaration of Competing Interest

The authors declare that they have no known competing financial interests or personal relationships that could have appeared to influence the work reported in this paper.

Acknowledgements

This work was supported by a University of Cyprus Internal Research Grant awarded to AJT. Work at the University of Florida was supported by National Science Foundation grant CHE-1900321.

Appendix A. Supplementary data

CCDC 2101802 and 2101674 contain the supplementary crystallographic data for compounds **1** and **2**, respectively. These data can be

obtained free of charge via http://www.ccdc.cam.ac.uk/conts/retrieving.html, or from the Cambridge Crystallographic Data Centre, 12 Union Road, Cambridge CB2 1 EZ, UK; fax: (+44) 1223-336-033; or e-mail: deposit@ccdc.cam.ac.uk. Supplementary material includes various structural and magnetism figures and tables. Supplementary data to this article can be found online at https://doi.org/10.1016/j.poly.2021.115551.

References

[1] C. Papatriantafyllopoulou, E.E. Moushi, G. Christou, A.J. Tasiopoulos, Filling the gap between the quantum and classical worlds of nanoscale magnetism: giant molecular aggregates based on paramagnetic 3d metal ions, Chem. Soc. Rev. 45 (6) (2016) 1597–1628, https://doi.org/10.1039/C5CS00590F.

[2] J. Fernando-Soria, J. Vallejo, M. Castellano, J. Martinez-Lillo, E. Pardo, J. Cano, I. Castro, F. Lloret, R. Ruiz-García, M. Julve, Molecular magnetism, quo vadis? A historical perspective from a coordination chemist viewpoint, Coord. Chem. Rev. 339 (2017) 17–103, https://doi.org/10.1016/j.ccr.2017.03.004.

[3] R. Bagai, G. Christou, The Drosophila of single-molecule magnetism: $[Mn_{12}O_{12}(O_2CR)_{16}(H_2O)_4]$, Chem. Soc. Rev. 38 (2009) 1011–1026, https://doi.org/10.1039/b811963e.

[4] C.J. Milios, R.E.P. Winpenny, Cluster-Based Single-Molecule Magnets, Struct. Bond. 164 (2015) 1–110, https://doi.org/10.1007/430_2014_149.

[5] D. Maniaki, E. Pilichos, S.P. Perlepes, Coordination Clusters of 3d-Metals That Behave as Single-Molecule Magnets (SMMs): Synthetic Routes and Strategies, Front. Chem. 6 (2018), https://doi.org/10.3389/fchem.2018.00461.

[6] T.C. Stamatatos, E. Rentschler, Organic chelate-free and azido-rich metal clusters and coordination polymers from the use of Me_3SiN_3: a new synthetic route to complexes with beautiful structures and diverse magnetic properties, Chem. Commun. 55 (1) (2019) 11–26, https://doi.org/10.1039/C8CC08854C.

[7] K.S. Pedersen, J. Bendix, R. Clérac, Single-molecule magnet engineering: building-block approaches, Chem. Commun. 50 (34) (2014) 4396–4415, https://doi.org/10.1039/C4CC00339J.

[8] W.-P. Chen, J. Singleton, L. Qin, A. Camón, L. Engelhardt, F. Luis, R.E.P. Winpenny, Y.-Z. Zheng, Quantum Monte Carlo simulations of a giant $\{Ni_{21}Gd_{20}\}$ cage with a S = 91 spin ground state, Nat. Commun. 9 (2018), https://doi.org/10.1038/s41467-018-04547-4.

[9] A.M. Ako, I.J. Hewitt, V. Mereacre, R. Clérac, W. Wernsdorfer, C.E. Anson, A. K. Powell, A Ferromagnetically Coupled Mn_{19} Aggregate with a Record S=83/2 Ground Spin State, Angew. Chem. Int. Ed. 45 (30) (2006) 4926–4929, https://doi.org/10.1002/anie.v45:3010.1002/anie.200601467.

[10] E.E. Moushi, T.C. Stamatatos, W. Wernsdorfer, V. Nastopoulos, G. Christou, A. J. Tasiopoulos, A Mn_{17} Octahedron with a Giant Ground-State Spin: Occurrence in Discrete Form and as Multidimensional Coordination Polymers, Inorg. Chem. 48 (12) (2009) 5049–5051, https://doi.org/10.1021/ic801795x.

[11] Y.-K. Deng, H.-F. Su, J.-H. Xu, W.-G. Wang, M. Kurmoo, S.-C. Lin, Y.-Z. Tan, J. Jia, D. Sun, L.-S. Zheng, Hierarchical Assembly of a $\{Mn^{II}_{15}Mn^{III}_{4}\}$ Brucite Disc: Step-by-Step Formation and Ferrimagnetism, J. Am. Chem. Soc. 138 (4) (2016) 1328–1334, https://doi.org/10.1021/jacs.5b11736.

[12] B.-Q. Ji, H.-F. Su, M. Jagodič, Z. Jagličić, M. Kurmoo, X.-P. Wang, C.-H. Tung, Z.-Z. Cao, D. Sun, Self-Organization into Preferred Sites by Mg^{II}, Mn^{II}, and Mn^{III} in Brucite-Structured M_{19} Cluster, Inorg. Chem. 58 (6) (2019) 3800–3806, https://doi.org/10.1021/acs.inorgchem.8b0340610.1021/acs.inorgchem.8b03406.s001.

[13] K.J. Mitchell, J.L. Goodsell, B. Russell-Webster, U.T. Twahir, A. Angerhofer, K. A. Abboud, G. Christou, Expansion of the Family of Molecular Nanoparticles of Cerium Dioxide and Their Catalytic Scavenging of Hydroxyl Radicals, Inorg. Chem. 60 (3) (2021) 1641–1653, https://doi.org/10.1021/acs.inorgchem.0c0313310.1021/acs.inorgchem.0c03133.s001.

[14] K.J. Mitchell, K.A. Abboud, G. Christou, Atomically-precise colloidal nanoparticles of cerium dioxide, Nat. Commun. 8 (2017), https://doi.org/10.1038/s41467-017-01672-4 article 1445.

[15] I.L. Malaestean, A. Ellern, P. Kögerler, $\{Ce_{10}Mn_8\}$: Cerium Analogues of the Decavanadate Archetype, Eur. J. Inorg. Chem. (2013) 1635–1638, https://doi.org/10.1002/ejic.201201247.

[16] A.B. Canaj, M. Siczek, T. Lis, M. Murrie, E.K. Brechin, C.J. Milios, A $[Ce_{21}]$ Keplerate, Dalton Trans. 46 (24) (2017) 7677–7680, https://doi.org/10.1039/C7DT01883E.

[17] A.E. Dearle, D.J. Cutler, H.W.L. Fraser, S. Sanz, E. Lee, S. Dey, I.F. Diaz-Ortega, G. S. Nichol, H. Nojiri, M. Evangelisti, G. Rajaraman, J. Schnack, L. Cronin, E. K. Brechin, An $[Fe^{III}_{34}]$ Molecular Metal Oxide, Angew. Chem. Int. Ed. 58 (47) (2019) 16903–16906, https://doi.org/10.1002/anie.v58.4710.1002/anie.201911003.

[18] A.E. Thuijs, X.-G. Li, Y.-P. Wang, K.A. Abboud, X.-G. Zhang, H.-P. Cheng, G. Christou, Molecular analogue of the perovskite repeating unit and evidence for direct Mn^{III}-Ce^{IV}-Mn^{III} exchange coupling pathway, Nat. Commun. 8 (2017), 500, https://doi.org/10.1038/s41467-017-00642-0.

[19] E.K. Brechin, Using tripodal alcohols to build high-spin molecules and single-molecule magnets, Chem. Commun. (2005) 5141–5153, https://doi.org/10.1039/b510102f.

[20] R. Inglis, C.J. Milios, L.F. Jones, S. Piligkos, E.K. Brechin, Twisted molecular magnets, Chem. Commun. 48 (2) (2012) 181–190, https://doi.org/10.1039/C1CC13558A.

[21] T.N. Nguyen, W. Wernsdorfer, K.A. Abboud, G. Christou, A Supramolecular Aggregate of Four Exchange-Biased Single-Molecule Magnets, J. Am. Chem. Soc. 133 (2011) 20688–20691, https://doi.org/10.1021/ja2087344.

[22] M. Manoli, R. Inglis, S. Piligkos, L. Yanhua, W. Wernsdorfer, E.K. Brechin, A. J. Tasiopoulos, A hexameric $[Mn^{III}_{18}Na_6]$ wheel based on $[Mn^{III}_{3}O]^{7+}$ sub-units, Chem. Commun. 52 (87) (2016) 12829–12832, https://doi.org/10.1039/C6CC06644E.

[23] H. Ida, T. Shiga, G.N. Newton, H. Oshio, Syntheses, structures and magnetism of mixed-valence Mn_{19} and Mn_{21} complexes supported by alkylamine-based alkoxo-bridging ligands, Inorg. Chem. Front. 2 (6) (2015) 538–543, https://doi.org/10.1039/C5QI00013K.

[24] M. Manoli, S. Alexandrou, L. Pham, G. Lorusso, W. Wernsdorfer, M. Evangelisti, G. Christou, A.J. Tasiopoulos, Magnetic "Molecular Oligomers" Based on Decametallic Supertetrahedra: A Giant Mn_{49} Cuboctahedron and its $Mn_{25}Na_4$ Fragment, Angew. Chem. Int. Ed. 55 (2) (2016) 679–684, https://doi.org/10.1002/anie.201509461.

[25] K. Skordi, C. Papatriantafyllopoulou, S. Zartilas, K.M. Poole, V. Nastopoulos, G. Christou, A.J. Tasiopoulos, Homometallic $\{Mn_{10}\}$ and heterometallic $\{Mn_6Ca_4\}$ supertetrahedra exhibiting an unprecedented $\{Mn^{III}_{9}Mn^{II}\}$ oxidation state level and heterometal ions distribution, Polyhedron 151 (2018) 433–440, https://doi.org/10.1016/j.poly.2018.05.029.

[26] M. Charalambous, E.E. Moushi, T.N. Nguyen, C. Papatriantafyllopoulou, V. Nastopoulos, G. Christou, A.J. Tasiopoulos, Giant Heterometallic $[Mn_{36}Ni_4]^{0/2-}$ and $[Mn_{32}Co_8]$ "Loops-of-Loops-and-Supertetrahedra" Molecular Aggregates, Front. Chem. 7 (2019), https://doi.org/10.3389/fchem.2019.00096.

[27] M. Charalambous, E.E. Moushi, C. Papatriantafyllopoulou, W. Wernsdorfer, V. Nastopoulos, G. Christou, A.J. Tasiopoulos, A $Mn_{36}Ni_4$ 'loop-of-loops-and-supertetrahedra' aggregate possessing a high $S_T = 26 \pm 1$ spin ground state, Chem. Comun. 48 (2012) 5410–5412, https://doi.org/10.1039/c2cc30654a.

[28] A.J. Tasiopoulos, A. Vinslava, W. Wernsdorfer, K.A. Abboud, G. Christou, Giant Single-Molecule Magnets: A $\{Mn_{84}\}$ Torus and Its Supramolecular Nanotubes, Angew. Chem. Int. Ed. 43 (16) (2004) 2117–2121, https://doi.org/10.1002/anie.200353352.

[29] A. Vinslava, A.J. Tasiopoulos, W. Wernsdorfer, K.A. Abboud, G. Christou, Molecules at the Quantum−Classical Nanoparticle Interface: Giant Mn_{70} Single-Molecule Magnets of ~4 nm Diameter, Inorg. Chem. 55 (7) (2016) 3419–3430, https://doi.org/10.1021/acs.inorgchem.5b02790.

[30] J.B. Vincent, H.-R. Chang, K. Folting, J.C. Huffman, G. Christou, D.N. Hendrickson, Preparation and Physical Properties of Trinuclear Oxo-Centered Manganese Complexes of the General Formulation $[Mn_3O(O_2CR)_6L_3]^{0,+}$ (R = Me or Ph; L = a Neutral Donor Group) and the Crystal Structures of $[Mn_3O(O_2CMe)_6(pyr)_3](pyr)$ and $[Mn_3O(O_2CPh)_6(pyr)_2(H_2O)]\cdot 0.5MeCN$, J. Am. Chem. Soc. 109 (1987) 5703–5711, https://doi.org/10.1021/ja00253a023.

[31] J.B. Vincent, C. Christmas, H.-R. Chang, Q. Li, P.D.W. Boyd, J.C. Huffman, D. N. Hendrickson, G. Christou, Modelling the Photosynthetic Water Oxidation Center. Preparation and Properties of Tetranuclear Manganese Complexes Containing $[Mn_4O_2]^{6+,7+,8+}$ Cores and the Crystal Structures of $Mn_4O_2(O_2CMe)_6(bipy)_2$ and $[Mn_4O_2(O_2CMe)_7(bipy)_2](ClO_4)$, J. Am. Chem. Soc. 111 (1989) 2086–2097, https://doi.org/10.1021/ja00188a023.

[32] T. Sala, M.V. Sargent, Tetrabutylammonium Permanganate: an Efficient Oxidant for Organic Substrates, J. Chem. Soc., Chem. Commun. (1978) 253–254, https://doi.org/10.1039/C39780000253.

[33] Oxford Diffraction, CrysAlis CCD and CrysAlis RED, version p171.38.46; Oxford Diffraction Ltd, Abingdon, Oxford, 2017.

[34] G.M. Sheldrick, SHELXT – Integrated space-group and crystal structure determination, Acta Crystallogr. Sect. A 71 (2015) 3–8, https://doi.org/10.1107/S2053273314026370.

[35] L.J. Farrugia, WinGX and ORTEP for Windows: an update, J. Appl. Crystallogr. 45 (4) (2012) 849–854, https://doi.org/10.1107/S0021889812029111.

[36] K. Brandenburg, DIAMOND. Version 3.1d. Crystal Impact GbR, Bonn, Germany, 2006.

[37] C.F. Macrae, P.R. Edgington, P. McCabe, E. Pidcock, G.P. Shields, R. Taylor, M. Towler, J. van de Streek, Mercury: visualization and analysis of crystal structures, J. Appl. Crystallogr. 39 (3) (2006) 453–457, https://doi.org/10.1107/S002188980600731X.

[38] A.L. Spek, PLATON SQUEEZE: a tool for the calculation of the disordered solvent contribution to the calculated structure factors, Acta Crystallogr, Sect. C 71 (2015) 9–18, https://doi.org/10.1107/S2053229614024929.

[39] M. Charalambous, S.M. Zartilas, E.E. Moushi, C. Papatriantafyllopoulou, M. J. Manos, T.C. Stamatatos, S. Mukherjee, V. Nastopoulos, G. Christou, A. J. Tasiopoulos, Discrete and encapsulated molecular grids: homometallic Mn_{15} and heterometallic $Mn_{24}Ni_2$ aggregates, Chem. Commun. 50 (65) (2014) 9090–9093, https://doi.org/10.1039/C4CC02893G.

[40] W. Liu, H.H. Thorp, Bond Valence Sum Analysis of Metal-Ligand Bond Lengths in Metalloenzymes and Model Complexes. 2. Refined Distances and Other Enzymes, Inorg. Chem. 32 (19) (1993) 4102–4105, https://doi.org/10.1021/ic00071a023.

[41] I.D. Brown, D. Altermatt, Bond-Valence Parameters Obtained from a Systematic Analysis of the Inorganic Crystal Structure Database, Acta Crystallogr, Sect. B 41 (4) (1985) 244–247, https://doi.org/10.1107/S0108768185002063.

[42] D. Savard, C. Cook, G.D. Enright, I. Korobkov, T.J. Burchell, M. Murugesu, Gradual spin crossover behaviour in a linear trinuclear Fe^{II} complex, CrystEngComm 13 (2011) 5190–5197, https://doi.org/10.1039/c1ce05275f.

[43] E.S. Koumousi, G. Lazari, S. Grammatikopoulos, C. Papatriantafyllopoulou, M. J. Manos, S.P. Perlepes, A.J. Tasiopoulos, G. Christou, T.C. Stamatatos, Rare nuclearities in Mn/oxo cluster chemistry: Synthesis and characterization of a mixed-valence $\{Mn^{II/III}_{11}\}$ complex bearing acetate and salicylhydroximate(-3)

bridging/chelating ligands, Polyhedron 206 (2021) 115298–115306, https://doi.org/10.1016/j.poly.2021.115298.
[44] S.P. Perlepes, J.C. Huffman, G. Christou, Preparation and Characterization of $[Mn_{11}O_{10}Cl_2(OAc)_{11}(bpy)_2(MeCN)_2(H_2O)_2](ClO_4)_2{\cdot}8MeCN$, a Mixed-valence Manganese(III/IV) Aggregate with Rare Undecanuclearity (bpy = 2,2'-bipyridyl), J. Chem. Soc., Chem. Commun. (1991) 1657–1659, https://doi.org/10.1039/C39910001657.
[45] S.M.J. Aubin, M.W. Wemple, D.M. Adams, H.-L. Tsai, G. Christou, D. N. Hendrickson, Distorted $Mn^{IV}Mn^{III}_3$ Cubane Complexes as Single-Molecule Magnets, J. Am. Chem. Soc. 118 (33) (1996) 7746–7754, https://doi.org/10.1021/ja960970f.
[46] W. Wernsdorfer, N. Aliaga-Alcalde, D.N. Hendrickson, G. Christou, Exchange-biased quantum tunnelling in a supramolecular dimer of single-molecule magnets, Nature 416 (6879) (2002) 406–409, https://doi.org/10.1038/416406a.
[47] K. Kambe, On the Paramagnetic Susceptibilities of Some Polynuclear Complex Salts, J. Phys. Soc. Jpn. 5 (1) (1950) 48–51, https://doi.org/10.1143/JPSJ.5.48.
[48] T.C. Stamatatos, K.A. Abboud, W. Wernsdorfer, G. Christou, "Spin Tweaking" of a High-Spin Molecule: An Mn_{25} Single-Molecule Magnet with an S=61/2 Ground State, Angew. Chem. Int. Ed. 46 (6) (2007) 884–888, https://doi.org/10.1002/(ISSN)1521-377310.1002/anie.v46:610.1002/anie.200603254.